The redox-active CXXC motif of BCAT1 regulates extracellular vesicle biogenesis in U937 macrophages

Experimental Cell Research 460 (2026) 115049

Contents lists available at ScienceDirect

Experimental Cell Research

journal homepage: www.elsevier.com/locate/yexcr

Research article

The redox-active CXXC motif of BCAT1 regulates extracellular vesicle biogenesis in U937 macrophages

James Hillier [a,*], Mathieu Y. Brunet [b], Rebecca Terry [c], Joanne Whittaker [c], Gemma Allcot [c], Sophie C. Cox [b], Patricia Esteban [b], Steven J. Coles [c,1], Ivan Wall [a,1]

[a] Immunology and Immunotherapy, University of Birmingham, Birmingham, B15 2TH, UK
[b] School of Chemical Engineering, University of Birmingham, Birmingham, B15 2TH, UK
[c] School of Science and the Environment, University of Worcester, Worcester, WR2 6AJ, UK

A B S T R A C T

Cytosolic branched-chain aminotransferase 1 (BCAT1) is a canonical transaminase that catalyses the breakdown of essential amino acids, including leucine, isoleucine and valine. Our previous work showed that BCAT1 also contains a redox-active CXXC motif with antioxidant activity, reducing intracellular reactive oxygen species (ROS) in the monocytic U937 cell line. Moreover, these cells display decreased expression of CD14/CD68 compared to controls, a phenotype indicative of M2 macrophage polarisation. Given that Extracellular Vesicle (EV) release is associated with oxidative stress, and that there is increasing interest in the therapeutic use of M1-and M2-derived macrophage EVs, we investigated whether the BCAT1 CXXC motif could modulate EV release in U937 cells constitutively overexpressing WT BCAT1, a CXXC motif mutant (CXXS BCAT1), or vector control. Here, we show that whilst WT BCAT1 cells display significantly lower intracellular ROS compared to controls, nanoparticle tracking analysis demonstrates that WT BCAT1 significantly increases EV generation compared to CXXS BCAT1 and vector controls under both normal (10% FBS) and serum-starved (0% FBS) conditions. Analysis of CD63/CD81/CD9 tetraspanin composition revealed that the majority of EVs produced were $CD63^+$, with serum starvation further increasing $CD63^+$ EV abundance. Taken together, these data indicate that BCAT1, and its redox-active CXXC motif, may play a novel role in EV biogenesis in macrophage-like cells.

1. Introduction

Extracellular vesicles (EVs) are a heterogeneous group of largely nano-meter scale membrane-bound vesicles released by a wide variety of cells that are broadly categorised by size and cellular origin [1] Several subtypes of EVs have been reported including large oncosomes (1000-10000 nm), apoptotic bodies (50-5000 nm), microvesicles (100-1000 nm) and exosomes (30-150 nm) [2,3]. Exosomes are released *via* intracellular multivesicular bodies (MVBs) which fuse with plasma membrane, whilst microvesicles and apoptotic bodies bud directly from the plasma membrane [4]. EVs have attracted significant interest in recent years due to their ability to deliver a range of bioactive cargo, including lipids, proteins and nucleic acids to recipient cells [5]. Importantly, EV composition reflects the physiological state of the parent cell, making them attractive both as biomarkers of disease and as potential therapeutic delivery vehicles [6–8].

In the context of macrophages, EVs have attracted increasing interest due to their role in regulating inflammatory responses. For example, there has been significant interest in EVs derived from anti-inflammatory (M2) macrophages for their therapeutic application in inflammatory diseases such as fibrosis and tissue repair [9]. Conversely, pro-inflammatory (M1) macrophage-derived EV's have also attracted attention as potential mediators in immunoregulation of infectious defence and cancers [10]. As such, understanding the mechanisms that govern EV biogenesis and composition in macrophages is of significant biological and therapeutic interest.

Cellular redox state is a key regulator of EV release [11]. For example, serum starvation, which causes an increase in mitochondrial derived ROS, has been shown to promote EV biogenesis [11,12]. Under these conditions, oxidative stress not only increases EV output but also alters EV cargo, reflecting activation of antioxidant and stress-response pathways. For example, the antioxidant stress response under control of Nuclear factor erythroid 2–related factor 2 (Nrf2), initiates the upregulation of antioxidant proteins such as Superoxide dismutase, peroxiredoxin and thioredoxin [13]. Kumar et. *al* used cigarette smoke condensate (CSC) exposure to induce oxidative stress in U937 cells [14]. This resulted in the packaging of proinflammatory cytokine IL-1β into extracellular vesicles, and target cells treated with these EVs showed

* Corresponding author.
E-mail addresses: j.hillier.2@bham.ac.uk, jameshillier@live.co.uk (J. Hillier).
[1] authors contributed equally to this study

https://doi.org/10.1016/j.yexcr.2026.115049
Received 20 January 2026; Received in revised form 21 April 2026; Accepted 28 April 2026
Available online 9 May 2026

increased IL-1β levels and antioxidant enzymes. Under oxidative stress, cellular antioxidant defences are eventually overwhelmed, and cells placed under serum starvation experience a significant loss of viability. For example, the monocytic U937 cell line is reported to lose approximately 80% viability between 48 and 72 h limiting the potential for continuous EV collection in long term cultures [15].

Mechanistically, redox regulation of EV release is linked to pathways controlling membrane trafficking and cytoskeletal dynamics [11]. For example, ROS have also been shown to directly regulate members of the RAS and Rab family of GTPases, which regulate membrane trafficking through a GXXXXGK(S/T)C motif, which contains a 'redox sensitive' C-terminal cysteine residue [16–18]. ROS can also modulate GTPAse activity indirectly through redox active protein tyrosine phosphatase (PTP) activity [19]. In addition, redox-sensitive proteins such as protein tyrosine phosphatases and thioredoxin have been implicated in EV biogenesis. A recent study found that exosome release from macrophages is regulated by SHP2 deactivation [20]. Moreover, SHP2 is positively regulated by the CXXC-motif containing oxidoreductase Thioredoxin (Trx), supporting the notion that EV release is a redox regulated process [21].

Cytosolic branched-chain aminotransferase (BCAT1) has gained significant interest in recent years that has largely focussed on its canonical metabolic role i.e., the reversible transfer of nitrogen from the branched-chain amino acids (BCAA) leucine, isoleucine, and valine to α-ketoglutarate, forming the respective branched-chain α-keto acid (BCKA) and glutamate [22,23]. However, BCAT1 also contains a redox active CXXC motif, and has redox midpoint potential similar to CXXC motif containing antioxidants such as Trx [24–26]. Our previous work has demonstrated that overexpression of BCAT1 in the myeloid cell line U937 reduces intracellular ROS in a CXXC-dependent manner, and also reduces CD14/CD68 expression in response to differentiation, indicating a more M2-like phenotype [27]. Moreover, studies in a neuronal cell model demonstrated BCAT1 CXXC motif dependant redox association with RhoGEF, which regulates the Rab and Ras GTPases, as well as numerous cytoskeletal proteins including tubulin, septin and myosin, all of which are involved in EV release [24,28]. Given the established links between redox signalling, mitochondrial metabolism, and EV biogenesis, these findings suggest that BCAT1 may act as a regulator of EV production in macrophage-like cells. Thus, the aim of this study was to investigate this potential role using our U937 cell model system [27].

2. Methods

2.1. Cell culture and reagents

U937 (ATCC® number CRL-1593.2TM) monocytic human myeloid leukaemia cell line was obtained from American Type Culture Collection (Glasgow, UK). U937 cells were maintained at 1×10^5 and 2×10^6 cells/mL, in RPMI-1640 media adjusted to contain 1% Penicillin/Streptomycin, 10% foetal bovine serum (FBS) and 2 mM L-glutamine. Cells were incubated at 37 °C and 5% CO_2.

2.2. Mutagenesis of BCAT1 and transduction in U937 cells

Site-directed mutagenesis of the BCAT1-CXXC motif and transduction into U937 cells was performed as previously described [27]. Stably transduced U937 cells overexpressing BCAT1 constructs were selected by incubation in complete RPMI supplemented with 0.5 μg/mL Puromycin. Constitutive overexpression of wild type (WT) BCAT1 and CXXS BCAT1 mutant was confirmed by qPCR with the following primers, Forward 5′-TGGAGAATGGTCCTAAGCTG-3′ and Reverse 5′-GC ACAATTGTCCAGTCGCTC 3′, with beta-2-microglobulin as a reference gene using the following primers, Forward 5′-ATGAGTATGCCTG CCGTGTGA-3′ and Reverse 5′-GGCATCTTCAAACCTCCATG-3′ as previously described [27].

2.3. Cell cycle, viability and morphology assessment

U937 cells were cultured in T75 flasks seeded at 2×10^5 cells/mL in a 10 mL total volume of complete RPMI for 72 h. Samples were taken at 24 h intervals. Cell size and granularity were assessed by forward scatter (FSC-H) and side scatter (SSC-H) profiling by flow cytometry. Cell density and viability were measured using Viacount stain (Merck-Millipore, London, UK) with the Easyfit Cluster Analysis Algorithm, using a Guava EasyCyte 6HT-2L flow cytometer (Merck-Millipore, London, UK). Cell size was assessed by light microscopy using the Las X software (Leica, Milton Keynes, UK). Exponential doubling time was calculated between 24 and 72 h. Cell cycle analysis of mid-exponential phase cells was performed by flow cytometry following propidium iodide staining after 48 h.

2.4. Intracellular ROS analysis

U937 cells were resuspend at a density of 1 x 10^6 cells/mL in 96-well plate and incubated for 24 h prior to analysis. Intracellular ROS was measured by flow cytometry following 2′,7′-dichlorofluorescein diacetate (DCFDA) staining using a DCFDA assay kit (Abcam, Cambridge, UK), in accordance with the manufacturer's instructions. Single cell analysis was performed using a fluorescence microscope and the Las X software (Leica, Milton Keynes, UK).

2.5. EV isolation

Culture medium utilised for EV isolation was depleted of FBS-derived EVs by ultracentrifugation at 120,000 g for 16 h prior to use. For EV harvesting, U937 cells were cultured in T75 flasks seeded at 8 x 10^5 cells/mL in a total of 20 mL complete RPMI supplemented with 10% EV-depleted FBS. Conditioned medium was collected every 2-3 days for a total of 10 days resulting in 4x 20 mL collections, 20 mL samples of conditioned medium was stored at −80 °C prior to consolidation and analysis. At each collection, cells were reseeded at 8 x 10^5 cells/mL in 20 mL of fresh media. EVs were isolated from conditioned medium (80 mL in total) by differential ultracentrifugation: 2000×*g* for 20 min, 10,000×*g* for 30 min and 120,000×*g* for 70 min. The supernatant was removed, and the EV containing pellet was washed in sterile PBS and centrifuged at 120,000×*g* for 70 min. The resultant pellet was re-suspended in 200 μl PBS for downstream analysis [29]. All ultracentrifugation steps were performed utilising the Sorvall WX Ultra Series Ultracentrifuge (Thermo Scientific, Oxford, UK) and a Fiberlite, F50L-8 × 39 fixed angle rotor (Piramoon Technologies Inc, Santa Clara, USA). Oxidative stress was induced by serum deprivation i.e., incubation with complete RPMI without FBS supplementation (0% FBS). Cells were incubated at a density of 1×10^6 cells per well in a 24 well plate in 1 mL complete RPMI without FBS for 24 h, at 37 °C and 5 % CO_2. The supernatant was harvested centrifuged twice at 2500×*g* for 15 min and filtered through a 0.45 μm sterile filter prior to analysis.

2.6. EV characterisation

Total EV protein concentration was determined using the Pierce bicinchoninic acid assay (BCA) kit (Thermo Scientific, Oxford, UK). Nanoparticle tracking analysis (NTA) was performed on EV samples to determine particle size and concentration using a Nanosight NS300 (Malvern Panalytical Ltd, Malvern, UK). Briefly, samples were diluted 1:100 in PBS and injected into the Nanosight, where 5x videos for 60 s were obtained of particles in motion. Particle size and concentration was determined with the Nanosight software according to the manufacturer's instructions (NanoSight NS300 User Manual, MAN0541-01-EN-00, 2017).

2.7. Immunofluorescent tetraspanin staining

Purified EVs isolated from conditioned media and EVs derived from serum free culture media were isolated as previously described and diluted 1/1000 and 1/2 in sample dilution buffer respectively. 50 µl was incubated on microarray chips pre-coated with anti-CD9, CD63 and -CD81 antibodies for 16 h overnight at room temperature as per manufacturer's instructions (Exoview Human Tetraspanin/Cargo kit. NanoView Biosciences, Boston, MA, USA). Briefly, samples were washed three times with 1000 µl 1X Solution A for 3 min with shaking followed by 10-min incubations with 250 µl of Solution C and Solution D with shaking. After each incubation, the samples were washed again three times with 1x Solution A. Samples were protected from light incubated with a 1:500 fluorescent antibody mixture containing anti-CD63 (CF®-647-labeled), anti-CD9 (CF®-488-labeled) and anti-CD81 (CF®-555-labeled) for 1 h. Following antibody incubation, samples were washed three times with 1000 µl 1X Solution A and Solution B for 3 min with shaking followed by washing with 1000 µl deionised (DI) water. Finally, microarray chips were transferred to a 10 cm Petri dish with filled with DI water and then removed to dry prior to detection using the Exoview platform. Fluorescent tetraspanin counts were directly exported from the ExoView Analyzer and analysed using GraphPad Prism v5.1.3 (Dotmatics; Boston, MA, USA).

2.8. Statistical analysis

Statistical significance was assessed by 1 and 2-way ANOVA and Bonferroni post-test for multiple comparisons, where a $p < 0.05$ was considered statistically significant. All data were analysed by GraphPad Prism v5.1.3.

3. Results

3.1. Overexpression of BCAT1 in U937 cells

Overexpression of BCAT1 in U937 cells was confirmed by qPCR which demonstrated a 20-25 -fold increase in both WT and CXXS BCAT1 mRNA transcripts with respect U937 cells vector control transgenic cells (Fig. 1. $P < 0.0001$). WT BCAT1 and CXXS BCAT1 expression was not significantly different, which allows effective evaluation of the relative contributions of the BCAT1 enzymatic/metabolic function, and the antioxidant CXXC motif (Fig. 1).

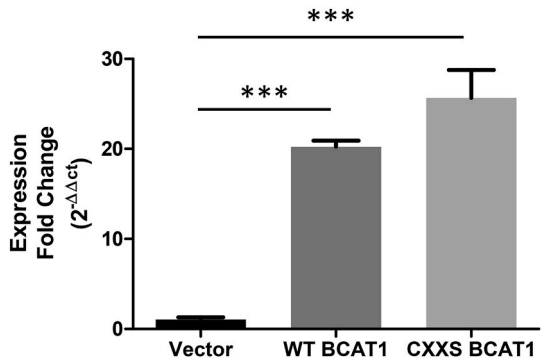

Fig. 1. BCAT1 overexpression in U937 cells Relative expression of presented as fold change in transgenic U937 cells compared to U937 control cells. Expression of BCAT1 to housekeeping gene B2M was calculated using the −2ΔΔCT method. Data presented are mean ± SD. Significant differences were calculated using 1-way ANOVA with Bonferroni post-test where * $p < 0.05$, ** $p < 0.01$, and *** $p < 0.001$. ($n = 3$).

3.2. BCAT1 expression decreases cell size and granularity

Since immune cell phenotype has been shown to change extracellular vesicle release and immune cell state and function has been linked to size and internal complexity/granularity, we next examined Forward Scatter (FSC-H) and Side Scatter (SSC-H) profiles by flow cytometry [30, 31]. BCAT1 over expressing cells displayed significantly reduced FSC-H profiles compared to control, indicating a reduction in cell size (Fig. 2b $p < 0.05$). Measurement of cell size by microscopic analysis confirmed WT BCAT1 cells had a smaller average size ($115.7 \pm 21.23\ \mu m^2$), compared to CXXS BCAT1 ($158.3 \pm 27.00\ \mu m^2$) and vector control ($170.5 \pm 30.15\ \mu m^2$) (Fig. 2d $p < 0.0001$). Moreover, BCAT1 overexpressing cells displayed significantly reduced SSC-H profiles (WT BCAT1 = 10639 ± 1668 MFI, CXXS BCAT1 = 11240 ± 213.4) compared to control (14372 ± 1668 MFI), indicating a reduction in internal complexity/granularity (Fig. 2c $p < 0.0001$). Taken together, this data shows WT BCAT1 cells display FSC/SSC profiles more indicative of pro-inflammatory or M1-type macrophages, which typically have increased size and granularity compared to anti-inflammatory M2 macrophages [32].

3.3. BCAT1 increases growth and viability BCAT1 in conditioned media

WT BCAT1, CXXS BCAT1 and vector control overexpressing U937 cells were grown in conditioned medium containing 10% EV depleted FBS. To ensure EVs were harvested from healthy cells, viability was assessed from 0 to 72 h. We have previously demonstrated this time frame corresponds to the exponential growth phase [27]. Flow cytometric analysis showed all cells exhibited 80-98% viability from 0 to 72 h (Fig. 3a), therefore EV containing media was harvested at 48-72 h (Fig. 3b). Fig. 3c shows WT BCAT1 (25.6 ± 1.4 h) and CXXS BCAT1 (27.4 ± 1.3 h) expressing cells display significantly reduced doubling time compared to the vector control (32.3 ± 3 0.1 h) in exponential phase growth (t = 24-72 h). Furthermore, average cell counts obtained from conditioned medium cultures where EVs were harvested were significantly increased for WT BCAT1 (1.28e+006 ± 550 cells/mL, $p < 0.05$) and CXXS BCAT1 (1.26e+006 ± 346 cells/mL, $p < 0.01$) expressing cells, relative to vector control (1.07e+006 ± 611 cells/mL). Cell cycle analysis revealed WT BCAT1 (23.2 ± 3.1 %, $p < 0.01$) and CXXS BCAT1 (23.7 ± 3.15 %, $p < 0.05$) cells display an increased proportion of G2M phase cells during the mid-exponential growth phase (t = 48), compared to Vector controls (16.4 ± 2.8 %) (Fig. 3e and f). This data shows that BCAT1 confers a growth and survival advantage in continuous flask cultures compared to controls.

3.4. BCAT1 reduces intracellular ROS in U937 cells in conditioned media and under serum starvation

Given EV release has been linked to oxidative stress, we next measured intracellular ROS using the DCFDA probe in U937 cells grown in conditioned medium containing 10% EV depleted FBS, as well as starvation (0% FBS) as previously described [27]. Flow cytometric analysis of cell culture in conditioned media reveals that DCFDA fluorescence intensity was significantly reduced in WT BCAT1 (154.3 ± 29.3 MFI, $p < 0.001$) and CXXS BCAT1 (159.0 ± 2.2 MFI) cells, compared to vector control (348.5 ± 20.5 MFI, Fig. 4a $p < 0.001$). Fluorescence microscopy confirms this observation, where WT BCAT1 (14.5 ± 3.8 MFI) and CXXS BCAT1 (13.0 ± 2.5 MFI) show a greater than 2-fold decrease in DCFDA signal, compared to vector controls (32.8 ± 4.6 MFI) (Fig. 3b $p < 0.0001$).

Serum starvation increased DCFDA signal in all cell lines. After 1 h of serum starvation, vector control cells had the highest DCFDA signal (530 ± 181 DCFDA MFI), while WT BCAT1 cells had the lowest (394.2 ± 89 DCFDA MFI), and CXXS BCAT1 cells showed an intermediate signal (464 ± 57 DCFDA MFI) (Fig. 4c $p < 0.005$). Interestingly, after 24 h, the difference in DCFDA signal between the groups

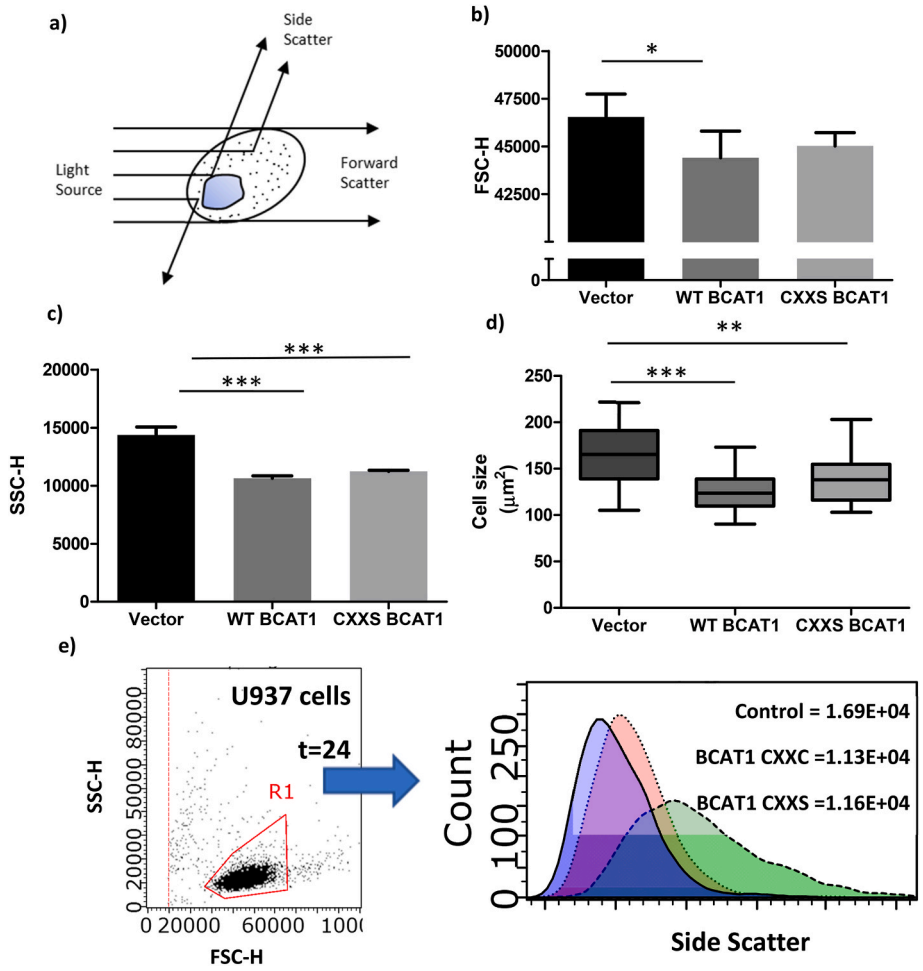

Fig. 2. BCAT1 over expression decreases cell size and granularity. a) Diagram representing flow cytometric assessment of cell size and granularity using the forward scatter (FSC-H) and side scatter (SSC-H) profiles. b + c) Flow cytometric analysis confirmed WT BCAT1 overexpressing cell display decreased forward scatter (FSC-H) and side scatter (SSC-H) profiles. d) Microscopic analysis of cell size confirm FSC-H analysis. e) Corresponding SSC-H histogram shows differences in morphology between cells. Data presented are mean ± SD. Significant differences were calculated using one-way ANOVA with Bonferroni post-test where * $p < 0.05$, ** $p < 0.01$, and *** $p < 0.001$ (n = 3).

(Vector > BCAT1-CXXS > WT BCAT1) was less pronounced, suggesting that cellular antioxidant defences may have activated during this period, reducing ROS levels. Fig. 4d shows these differences visualised in representative flow cytometric histograms. Analysis of DCFDA stained cells by fluorescence microscopy reflect the flow cytometric data, where WT BCAT1 displays lower DCFDA signal than CXXS BCAT1 cells or vector controls. Moreover, WT BCAT1 cells, show regional 'ROS hotspots' at the periphery, which indicate localised ROS increases close to the cell membrane following serum starvation (Fig. 4e.). In summary, WT BCAT1 displays significantly lower intracellular ROS compared to BCAT1 CXXS and vector controls in conditioned media and under serum starvation. Serum starvation increases intracellular ROS with localised ROS hotspots close to the cell surface, which appears to impact morphology in BCAT1 overexpressing cells.

3.5. BCAT1 expression increases EV release

Next, we examined the effect of BCAT1 expression and the relative contribution of the CXXC motif on EV release by Nanoparticle tracking analysis, using purified EVs harvested from conditioned media (10% FBS) and non-purified EVs harvested from serum free media (0% FBS). In conditioned medium containing (10% FBS), NTA measurements show WT BCAT1 overexpressing cells display approximately 5-fold increase in normalised EV count (3012 ± 258 EVs/cell) compared to vector controls (639.1 ± 62 EVs/cell, $p < 0.0001$), and a 2-fold increase compared to CXXS BCAT1 (1683 ± 178 EVs/cell) (Fig. 5a and b). This trend is reflected in total protein content of EV samples measure by the BCA assay, where WT BCAT1 EV samples have an increased protein content (120.5 ± 2.1 µg/mL) compared to BCAT1-CXXS (95.1 ± 8.9 µg/mL) and vector controls (107 ± 2.1 µg/mL) (Supplementary Fig. 1). Size distribution analysis of EVs harvested from conditioned media shows WT BCAT1 and CXXS BCAT1 expression resulted in significantly decreased average EV diameter (145.5 ± 3.40 nm, 147.9 ± 15.75 nm) compared to controls (202.7 ± 8.17 nm) (Fig. 5d $p < 0.0001$). Following serum starvation (0% FBS), NTA measurement shows the same pattern where WT BCAT1 overexpressing cells release an increased amount of smaller EVs (5.41e+08 ± 5.29e+07 particles/ml) compared to vector controls (3.62e+08 ± 4.25e+07 particles/ml), or CXXS BCAT1 cells (4.16e+08 ± 1.47e+07 particles/ml) (Fig. 5a and c, $P < 0.0001$).

3.6. BCAT1 expression increases $CD63^+$ EV release

The Exoview R100 platform (Nanoview bioscience) allows for immunofluorescent detection and visualisation of EVs incubated on a microarray of anti-CD9, CD63 and CD81. Data presented show capture spots isolated from conditioned media, and serum starved media (Fig. 6a and b). Analysis of EVs harvested from conditioned media reveal that WT BCAT1 expressing cells display significantly increased EV counts

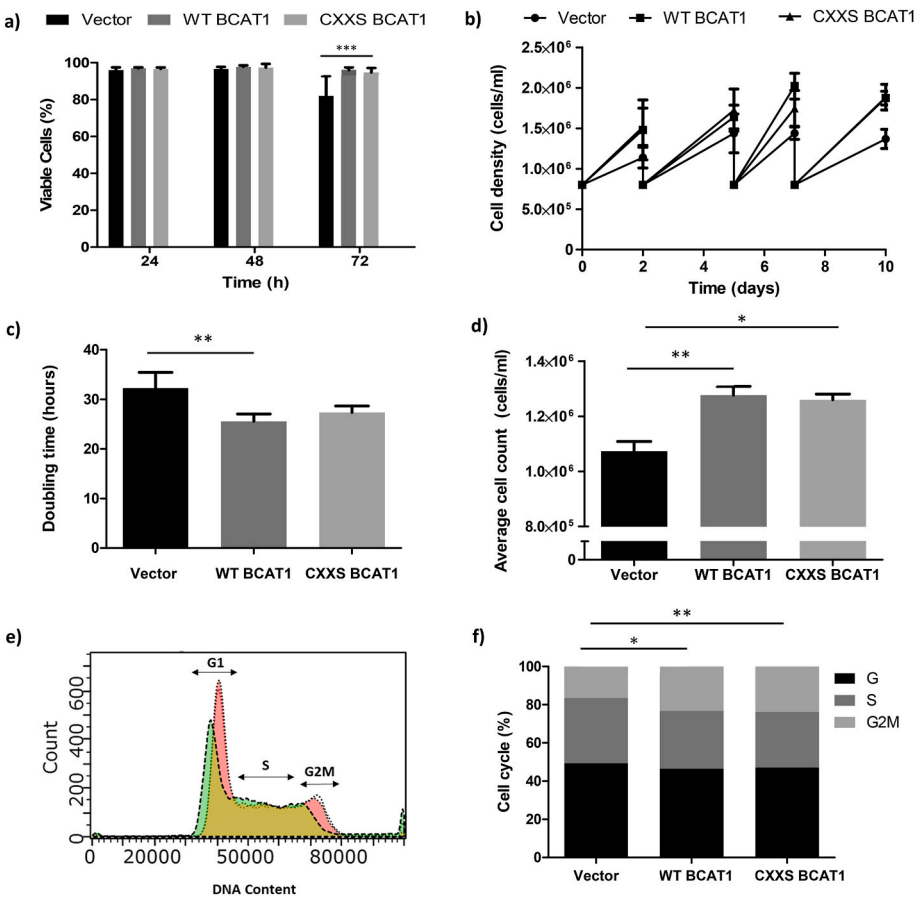

Fig. 3. BCAT1 increases growth and viability BCAT1 in conditioned media. a) Cell viability from 0 to 72 h across cell lines. b) Cell density of U937 cells over-expressing WT BCAT1, CXXS BCAT1 and Vector over 0–240 h measured by flow cytometry. Supernatant containing extracellular vesicles was harvested every 2-3 days and cells were resuspended in fresh RPMI +10% EV-depleted FBS at 8 x 10^5 cells/ml. c) BCAT1 overexpressing cells display reduced doubling time 24-72 h and d) reached a higher average cell number over the time course e) cell cycle analysis at t = 48 h reveals BCAT1 cells have a higher proportion of G2M phase cells than controls. WT BCAT1 (No fill) and CXXS BCAT1, Vector Control (Green fill). f) WT BCAT1 and CXXS BCAT1 display a significantly reduced proportion of G2M phase cells compared to vector controls. Data presented are mean ± SD. Significant differences were calculated using ANOVA with Bonferroni post-test where * $p < 0.05$, ** $p < 0.01$, and *** $p < 0.001$. (n = 3).

(1514 ± 386 $CD63^+$ EVs) captured by anti-CD63 compared to CXXS BCAT1 (603 ± 399 $CD63^+$ EVs) and Vector control (101 ± 27 $CD63^+$ EVs) ($P < 0.0001$). EVs captured by CD9 and CD81 were not significantly different compared to IgG controls in any cell line. Under serum starved conditions, EVs captured by CD63 were increased compared to conditioned media samples. Under these conditions, WT BCAT1 continued to show significantly increased EV counts (3934 ± 198 EVs) compared to vector controls (2631 ± 329 EVs) and CXXS BCAT1 (3289 ± 119 EVs) ($P < 0.0001$). CD81 and CD9 expression remained unchanged compared to IgG controls. Taken together, this data shows that WT BCAT1 expression increases $CD63^+$ EV release in both serum conditions compared to vector control and CXXS BCAT1, indicating a role for the CXXC motif in this process (Fig. 7).

4. Discussion

This study has examined the effect of BCAT1 and its antioxidant CXXC motif on the release of EVs in the myeloid cell line U937 cells. This experimental design stems from previous studies that demonstrated that EV release is at least a partially redox-mediated process and can be elicited through serum starvation, which results in mitochondrial ROS production [33]. Given our previous work which demonstrated that the BCAT1 CXXC motif reduces intracellular ROS, and increases cell viability in response to serum starvation, we hypothesised that WT BCAT1 expression could alter extracellular vesicle release [27].

To investigate this, we utilised U937 cells modified to overexpress WT BCAT1 and CXXS BCAT1 mutant protein, where the C-terminal cysteine thiol (-SH) has been mutagenized to serine (-OH). Our previous work demonstrated that this alteration abolishes the CXXC motif antioxidant capacity *in vitro*, as the C-terminal cysteine can no longer function as the 'resolving' cysteine in the dithiol-disulphide exchange reaction [27]. This mechanism is typical of CXXC-containing antioxidant enzymes such as thioredoxin [34]. Importantly, to allow discrimination of metabolic activity and CXXC motif antioxidant effects, CXXS BCAT1 retains its enzymatic capacity *in vivo*, where the N-terminal cysteine becomes S-glutathionylated under physiological conditions protecting it from further oxidation [24]. Overexpression of BCAT1 in U937 cells was confirmed by qPCR, which demonstrated significant fold expression change of both WT BCAT1 and CXXS BCAT1 compared to vector control (Fig. 1). Importantly WT BCAT1 and CXXS BCAT1 expression were not significantly different, which allows effective evaluation of the relative contributions of the BCAT1 enzymatic/metabolic function and the antioxidant CXXC motif.

The induction of oxidative stress through serum starvation is a commonly used technique to increase cellular EV generation [35]. Therefore, intracellular ROS was measured by the DCFDA probe from cells cultured with conditioned media (10% EV-depleted FBS) and under serum starvation (0% FBS). The data show serum starvation increases ROS across all cell lines. However, WT BCAT1 cells display lower intracellular ROS compared to CXXS BCAT1 and vector control under

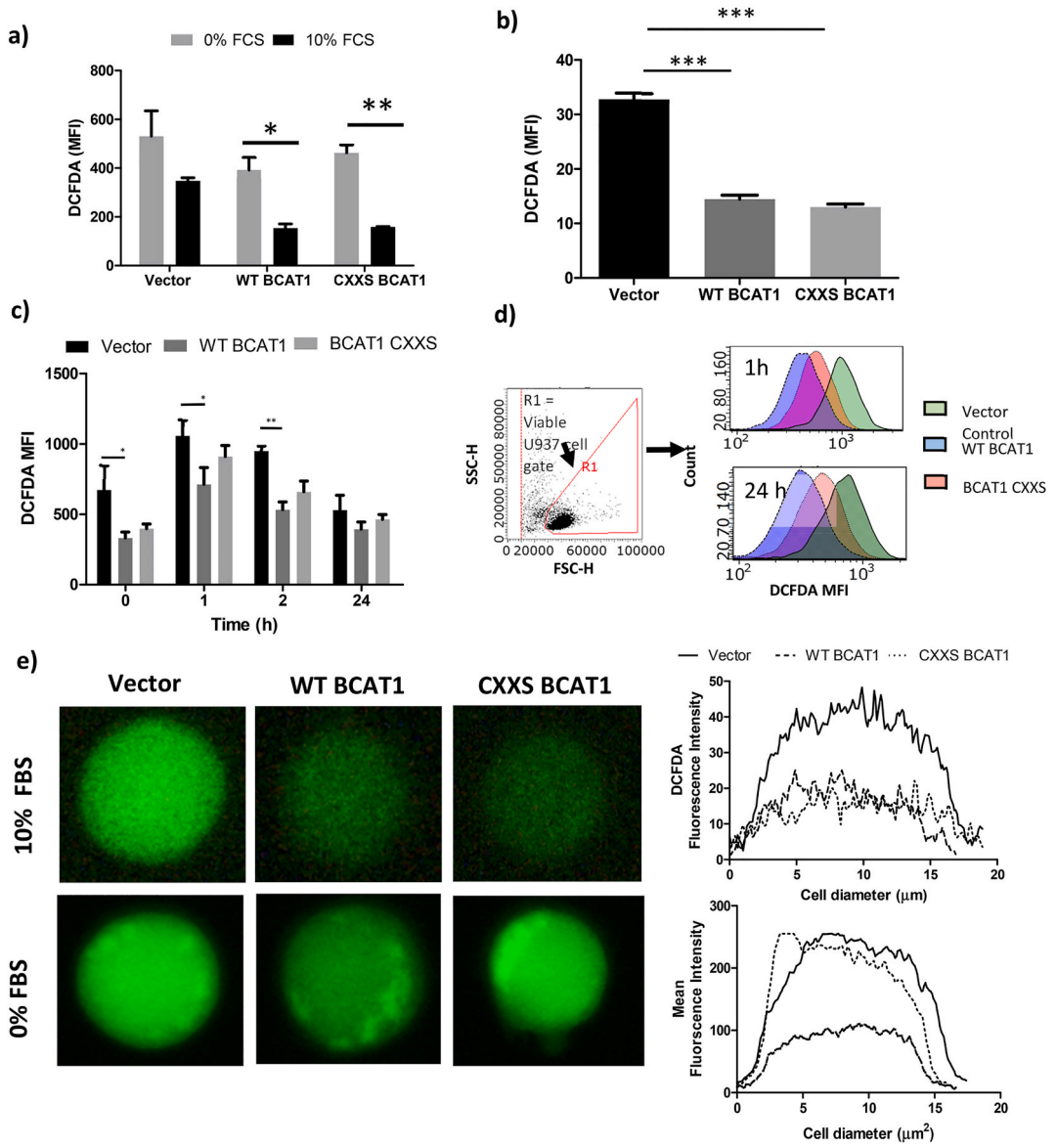

Fig. 4. BCAT1 reduces intracellular ROS in U937 cells in conditioned media and under serum starvation. Cells were incubated for 1 h in 96 well plates seeded at 100 000 cells/well with complete RPMI and 0-10% FBS. a) Serum starvation (0% FBS) increases DCFDA compared to control (10% FBS) in vector control, WT BCAT1 and CXXS BCAT1 cells. b) Analysis by fluorescent microscopy confirmed WT BCAT1 and CXXS display significantly lower DCFDA compared to Vector control in 10% FBS. c) DCFDA signal increases over time in response to serum starvation d) Representative flow cytometric histogram overlays of serum starvation at 1 h and 24 h where ROS Vector > CXXS BCAT1>WT BCAT1 e) Fluorescent images (x40 magnification) and cross-sectional analysis at 10% and 0% FBS. Interestingly cells appear to show regional ROS 'hotspots' at cell periphery at 0% FBS. Data presented as mean ± SD. Significant differences were calculated using 2-way ANOVA with Bonferroni post-test where * $p < 0.05$, ** $p < 0.01$, and *** $p < 0.001$ (n = 3).

normal (10% FBS) and serum starved (0% FBS) media conditions (Fig. 4, $p < 0.01$).

Next, EV release was compared across WT BCAT, CXXS BCAT1 and vector controls in conditioned media and under serum starvation. Nanoparticle tracking analysis (NTA) of EVs from conditioned media shows WT BCAT1 expression significantly increases EVs released per cell compared to CXXS BCAT1 and vector controls (Fig. 5b, $p < 0.0001$). Moreover, NTA analysis of EVs harvested following serum starvation showed the same pattern, thus indicating that EV biogenesis in this model is not solely driven by oxidative stress, but may instead reflect underlying metabolic or mitochondrial regulation (Fig. 5c, $p < 0.0001$).

To corroborate the NTA data, tetraspanin composition was evaluated. EV samples were analysed using the Exoview platform. EVs harvested from conditioned media and serum starved conditions showed no significant expression of CD81 or CD9 across all cell lines, confirming previous reports that U937 cells exhibit minimal CD81 and CD9 expression [36], WT BCAT1 samples showed a significant increase in CD63-positive EVs, and serum starvation induced a marked increase in CD63-positive vesicles across all conditions (Figs. 6 and 7). The observation that WT BCAT1 overexpressing cells release more EVs may be explained by BCAT1 enzymatic products, which include α-ketoglutarate and leucine, both of which have been shown to mediate EV release [37, 38]. Moreover, α-ketoglutarate feeds directly into the tricarboxylic acid (TCA) cycle, where mitochondrial and TCA cycle dysfunction are known to influence redox balance and cellular signalling and are increasingly recognised as regulators of extracellular vesicle biogenesis [39]. It is therefore plausible that BCAT1 modulates EV production through metabolic regulation of mitochondrial function rather than ROS alone. Disruption of mitochondrial homeostasis - including altered oxidative phosphorylation, impaired quality control, and dysregulated metabolite

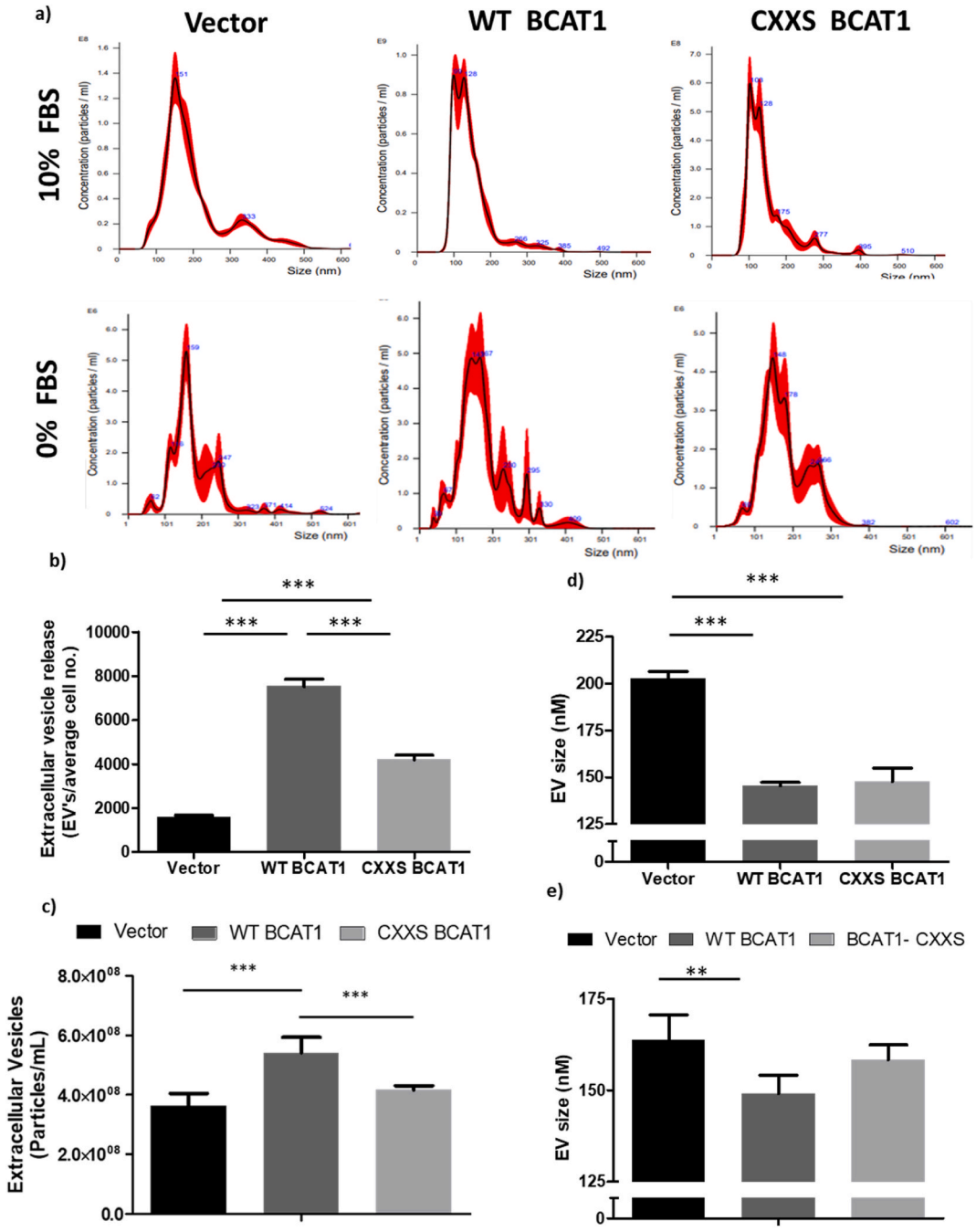

Fig. 5. Extracellular vesicle release differs dependant BCAT1 expression and CXXC motif. a) Nanoparticle tracking analysis (NTA) shows distinct profiles for EVs harvested under 10% and 0% FBS. EVs harvested from b) 10% FBS and c) 0% FBS show the number of EVs released vary with BCAT1 expression and the mutational status of the CXXC motif where WT BCAT1 > CXXS BCAT1 > Vector control. NTA size analysis reveals WT BCAT1 and BCAT1 CXXS EVs are smaller in size than vector controls in both d) 10% FBS and e) 0% FBS. Data presented are mean ± SD. Significant differences were calculated using ANOVA with Bonferroni post-test where * $p < 0.05$, ** $p < 0.01$, and *** $p < 0.001$. ($n = 3$).

flux - has been implicated in a range of pathological states, particularly cardiovascular and endothelial injury, where targeting mitochondrial pathways can attenuate tissue damage [40–42]. In this context, modulation of mitochondrial redox balance and antioxidant pathways has emerged as a key strategy to restore cellular homeostasis and limit tissue injury [43]. Moreover, in immune cells, mitochondrial metabolism is a key determinant of macrophage polarisation, with TCA cycle intermediates acting as signalling molecules that regulate inflammatory responses [44,45]. However, our data indicate that EV production is also dependent on CXXC motif status, as CXXS BCAT1 cells displayed reduced vesicle numbers compared to WT BCAT1. The mechanism by which the CXXC motif influences EV release remains unclear. Previous studies have demonstrated the BCAT1 CXXC motif forms redox interactions with RhoGEF, as well as numerous cytoskeletal proteins including tubulin, septin and myosin, all of which are also involved in EV release [24,28]. Cytoskeletal processes such as actin polymerisation and severing are also directly involved in microvesicle release, which bud from the plasma membrane [46]. Whilst the involvement of these cytoskeletal rearrangements are less clear for the formation of smaller vesicles like exosomes, actin and related proteins such as the contractile protein myosin, are amongst the most abundant proteins that make up EVs, thus demonstrating their importance to EV biogenesis [47]. Thus it

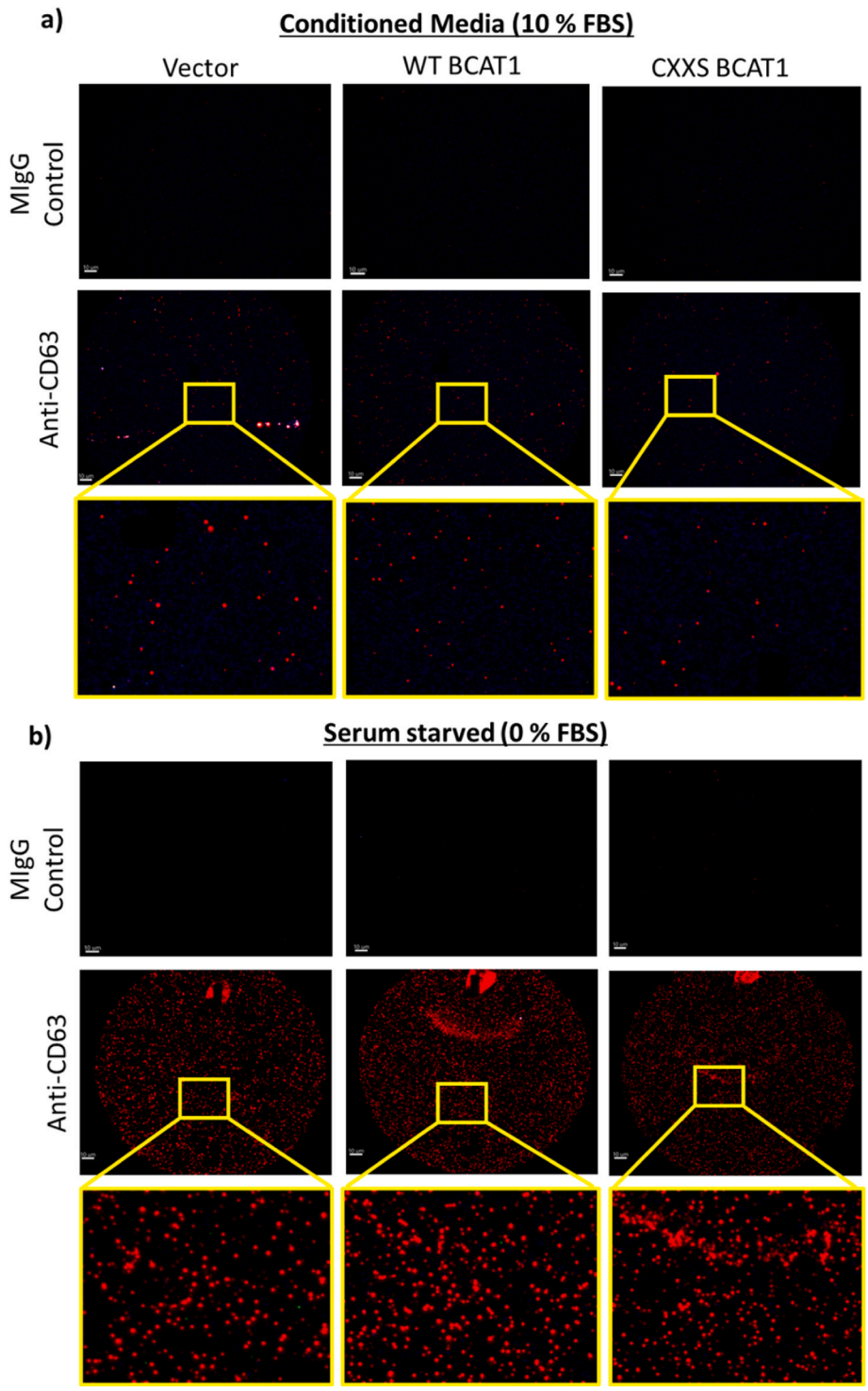

Fig. 6. Extracellular vesicles captured and fluorescently labeled using ExoView platform. EVs are immobilised on anti-CD63 or Mouse IgG control capture spots and stained with fluorescently labeled tetraspanin markers CD63 (red), C81 (green) and CD9 (blue) antibodies. Representative images of U937 derived EV harvested from a) conditioned medium containing 10% EV-depleted FBS and b) serum starved media (0% FBS).

is possible that redox sensitive cytoskeletal proteins or their binding partners/regulators interact with the CXXS BCAT1 protein through the intact N-terminal cysteine, however without the C-terminal resolving cysteine these proteins bind irreversibly disrupting cytoskeletal processes or signalling pathways involved in EV biogenesis at the plasma membrane. Our preliminary supports this notion, indicating that the BCAT1 CXXC motif status alters cofilin oligomerisation which regulates actin polymerisation, suggesting that BCAT1 could play a role in cytoskeletal remodelling and therefore EV release [48]. Given that BCAT1 enzymatic activity is pharmacologically targetable, for example using inhibitors such as gabapentin, this raises the possibility that BCAT1 may represent a novel entry point for modulating mitochondrial/metabolic/cytoskeletal pathways that influence EV biogenesis and macrophage function [49].

Analysis of size and morphology revealed that WT BCAT1 cells displayed a smaller, more spherical morphology than either vector control

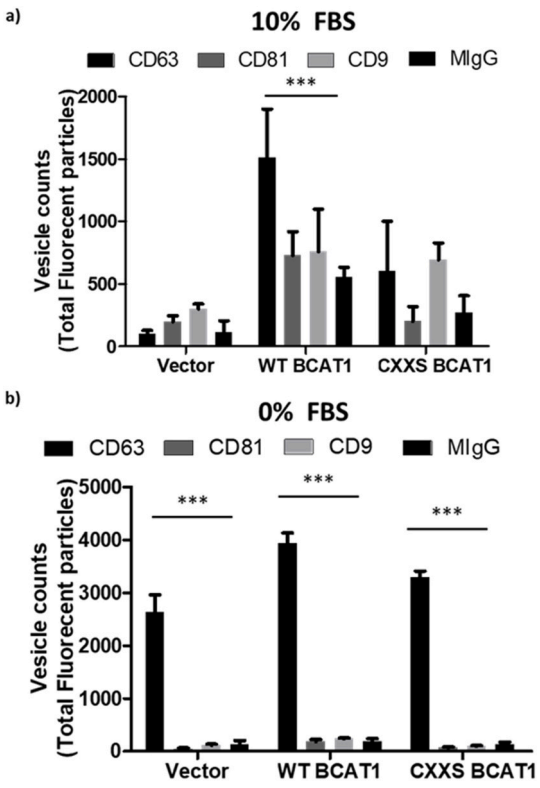

Fig. 7. BCAT1 expression increases CD63$^+$ EV release. Immunofluorescent detection of EVs incubated on a microarray of antibody spots against CD9, CD63 and CD81 shows a) EVs harvested from conditioned media (10% FBS) reveal WT BCAT1 expressing cells display significantly increased EV counts (1514 ± 386 CD63$^+$ EVs) compared to CXXS BCAT1 (603 ± 399 CD63$^+$ EVs) and Vector control (101 ± 27 CD63$^+$ EVs). b) Serum starvation (0% FBS) results in a large increase in the proportion of CD63$^+$ EVs across all cell lines. Of these WT BCAT1> CXXS BCAT1> Vector control in terms of EV released. Significant differences were calculated using ANOVA with Bonferroni post-test where * $p < 0.05$, ** $p < 0.01$, and *** $p < 0.001$. ($n = 3$).

or CXXS BCAT1. Flow cytometric analysis confirmed reduced forward (FSC) and side scatter (SSC), indicating decreased size and granularity (Fig. 2). Previous studies have found that flow cytometric scatter profiles are correlated to immune cell function, and this includes macrophages which display increased size and granularity upon differentiation [31, 50]. Pro-inflammatory or M1-type macrophages, typically have increased size and granularity as measured by FSC and SSC compared to anti-inflammatory M2 macrophages [32]. Thus, our findings indicate that WT BCAT1 overexpressing cells are more M2-like in FSC/SSC phenotype. This confirms observations from our previous work, which showed WT BCAT1 U937 cells display a more M2 like signature, showing reduced CD14/CD68 expression compared to CXXS BCAT1 and vector Controls [27]. EVs derived from M1/M2 macrophages have attracted significant attention for their therapeutic potential in numerous, diseases by delivering a bioactive cargo that reflects the parent cell [9]. For example, in the context of wound healing, initially M1 macrophages are recruited to a site of infection to deliver pro-inflammatory cargo that sterilises the wound before transitioning to M2 macrophages that deliver anti-inflammatory cargo that promotes wound repair [51]. Therefore, EVs derived from M1/M2 macrophages may be useful therapeutics to manipulate wound dynamics. This would be particularly useful in the case of chronic wounds, for example diabetic foot ulcers which are associated with chronic inflammation [52]. Given that our data indicate that WT BCAT1 overexpressing cells display a more 'M2 like' phenotype, it may represent an attractive target to manipulate M2 polarisation. In this context, one approach could involve the local delivery of BCAT1 or modulating agents such as gabapentin *via* lipid nanoparticle (LNP) encapsulation within hydrogel-based wound dressings, to influence macrophage metabolism and phenotype directly at the site of injury. Lipid nanoparticle delivery systems have been successfully used to mitigate mitochondrial dysfunction in other disease models; however, several key questions must be addressed to support the feasibility of this approach as a future medical development [53]. First, this study utilises the U937 cell line, which may not fully recapitulate primary human macrophage biology, and therefore requires validation in primary cells and *in vivo* models. In addition, while EV quantity and surface marker composition were assessed, their molecular cargo remains undefined. As EV function is highly dependent on cargo, future studies should determine how BCAT1 influences EV composition and the downstream effects on recipient cells. Furthermore, the mechanistic link between the CXXC motif and EV biogenesis remains indirect and will require a targeted investigation of cytoskeletal and mitochondrial signalling pathways.

In summary, WT BCAT1 significantly increases EV generation compared to CXXS BCAT1 and vector controls under both normal and serum-starved conditions, despite reducing intracellular ROS. These findings support a model in which BCAT1 regulates EV biogenesis through an interplay between metabolic activity, mitochondrial function, and redox signalling. Taken together, this work identifies BCAT1 and its CXXC motif as novel regulators of EV production in macrophage-like cells and highlights their potential relevance in both disease biology and EV-based therapeutic strategies.

CRediT authorship contribution statement

James Hillier: Conceptualization, Data curation, Formal analysis, Investigation, Writing – original draft, Writing – review & editing. **Mathieu Y. Brunet:** Investigation, Methodology, Writing – review & editing. **Rebecca Terry:** Investigation. **Joanne Whittaker:** Supervision. **Gemma Allcot:** Investigation. **Sophie C. Cox:** Resources, Supervision. **Patricia Esteban:** Supervision, Writing – review & editing. **Steven J. Coles:** Conceptualization, Funding acquisition, Methodology, Resources, Supervision, Writing – review & editing. **Ivan Wall:** Funding acquisition, Supervision.

Declaration of competing interest

The authors declare that they have no known competing financial interests or personal relationships that could have appeared to influence the work reported in this paper.

Appendix A. Supplementary data

Supplementary data to this article can be found online at https://doi.org/10.1016/j.yexcr.2026.115049.

Data availability

Data will be made available on request.

References

[1] E. Willms, C. Cabañas, I. Mäger, M.J.A. Wood, P. Vader, Extracellular vesicle heterogeneity: subpopulations, isolation techniques, and diverse functions in cancer progression, Front. Immunol. 9 (2018) 355368, https://doi.org/10.3389/FIMMU.2018.00738/BIBTEX.
[2] L.M. Doyle, M.Z. Wang, Overview of extracellular vesicles, their origin, composition, purpose, and methods for exosome isolation and analysis, Cells 8 (2019), https://doi.org/10.3390/CELLS8070727.
[3] V.R. Minciacchi, S. You, C. Spinelli, S. Morley, M. Zandian, P.-J. Aspuria, L. Cavallini, C. Ciardiello, M.R. Sobreiro, M. Morello, G. Kharmate, S.C. Jang, D.-K. Kim, E. Hosseini-Beheshti, E.T. Guns, M. Gleave, Y.S. Gho, S. Mathivanan, W. Yang, M.R. Freeman, D. Di Vizio, Large oncosomes contain distinct protein cargo and represent a separate functional class of tumor-derived extracellular vesicles, Oncotarget 6 (2015) 11327–11341, https://doi.org/10.18632/oncotarget.3598.

[4] E.R. Abels, X.O. Breakefield, Introduction to extracellular vesicles: biogenesis, RNA cargo selection, content, release, and uptake, Cell. Mol. Neurobiol. 36 (2016) 301–312, https://doi.org/10.1007/s10571-016-0366-z.

[5] B. Mir, C. Goettsch, Extracellular vesicles as delivery vehicles of specific cellular cargo, Cells 9 (2020) 1601, https://doi.org/10.3390/cells9071601.

[6] F. Urabe, N. Kosaka, K. Ito, T. Kimura, S. Egawa, T. Ochiya, Extracellular vesicles as biomarkers and therapeutic targets for cancer, extracellular vesicles in cell, Physiol.Am. J. Physiol. Cell Physiol. 318 (2020) 29–39, https://doi.org/10.1152/ajpcell.

[7] M.C. Ciferri, R. Quarto, R. Tasso, S. Bernardi, Biology extracellular vesicles as biomarkers and therapeutic tools: from pre-clinical to clinical applications. https://doi.org/10.3390/biology, 2021.

[8] C. Ay, J. Thaler, A. Georgescu, R.R. Koenen, A. Dickhout, Extracellular vesicles as biomarkers in cardiovascular disease; chances and risks, Front. Cardiovasc. Med.¦ Www.Frontiersin.Org 1 (2018) 113, https://doi.org/10.3389/fcvm.2018.00113.

[9] Y. Wang, M. Zhao, S. Liu, J. Guo, Y. Lu, J. Cheng, J. Liu, Macrophage-derived extracellular vesicles: diverse mediators of pathology and therapeutics in multiple diseases, Cell Death Dis. 11 (2020) 924, https://doi.org/10.1038/s41419-020-03127-z.

[10] L. Cheng, Y. Wang, L. Huang, Exosomes from M1-Polarized macrophages potentiate the cancer vaccine by creating a pro-inflammatory microenvironment in the lymph node, Mol. Ther. 25 (2017) 1665–1675, https://doi.org/10.1016/j.ymthe.2017.02.007.

[11] E. Chiaradia, B. Tancini, C. Emiliani, F. Delo, R.M. Pellegrino, A. Tognoloni, L. Urbanelli, S. Buratta, Extracellular vesicles under oxidative stress conditions: biological properties and physiological roles, Cells 10 (2021) 1763, https://doi.org/10.3390/cells10071763.

[12] F. Wang, R.A. Cerione, M.A. Antonyak, Isolation and characterization of extracellular vesicles produced by cell lines, STAR Protoc. 2 (2021) 100295, https://doi.org/10.1016/j.xpro.2021.100295.

[13] M. Jaganjac, L. Milkovic, S.B. Sunjic, N. Zarkovic, The NRF2, thioredoxin, and glutathione system in tumorigenesis and anticancer therapies, Antioxidants 9 (2020) 1151, https://doi.org/10.3390/antiox9111151.

[14] S. Kodidela, N. Sinha, A. Kumar, L. Zhou, S. Godse, S. Kumar, Extracellular vesicles released from macrophages modulates interleukin-1β in astrocytic and neuronal cells, Sci. Rep. 13 (2023) 3005, https://doi.org/10.1038/s41598-023-29746-y.

[15] G. Birarda, D.E. Bedolla, E. Mitri, S. Pacor, G. Grenci, L. Vaccari, Apoptotic pathways of U937 leukemic monocytes investigated by infrared microspectroscopy and flow cytometry, Analyst 139 (2014) 3097–3106, https://doi.org/10.1039/C4AN00317A.

[16] J. Heo, S.L. Campbell, Mechanism of redox-mediated guanine nucleotide exchange on redox-active rho GTPases, J. Biol. Chem. 280 (2005) 31003–31010, https://doi.org/10.1074/jbc.M504768200.

[17] A. Aghajanian, E.S. Wittchen, S.L. Campbell, K. Burridge, Direct activation of RhoA by reactive oxygen species requires a redox-sensitive motif, PLoS One 4 (2009) e8045, https://doi.org/10.1371/journal.pone.0008045.

[18] E. Ferro, L. Goitre, S.F. Retta, L. Trabalzini, The interplay between ROS and ras GTPases: physiological and pathological implications, J. Signal Transduct. 2012 (2012), https://doi.org/10.1155/2012/365769.

[19] A.S. Nimnual, L.J. Taylor, D. Bar-Sagi, Redox-dependent downregulation of rho by rac, Nat. Cell Biol. 5 (2003) 236–241, https://doi.org/10.1038/ncb938.

[20] Y. Zhang, Y. Li, P. Liu, D. Gong, H. Zhou, W. Li, H. Zhang, W. Zheng, J. Xu, H. Cheng, X. Zhang, Y. Ke, Phosphatase Shp2 regulates biogenesis of small extracellular vesicles by dephosphorylating syntenin, J. Extracell. Vesicles 10 (2021), https://doi.org/10.1002/JEV2.12078.

[21] C.-Y. Chen, D. Willard, J. Rudolph, Redox regulation of SH2-domain-containing protein tyrosine phosphatases by two backdoor cysteines, Biochemistry 48 (2009) 1399–1409, https://doi.org/10.1021/bi801973z.

[22] Y. Xu, W. Yu, T. Yang, M. Zhang, C. Liang, X. Cai, Q. Shao, Overexpression of BCAT1 is a prognostic marker in gastric cancer, Hum. Pathol. 75 (2018) 41–46, https://doi.org/10.1016/j.humpath.2018.02.003.

[23] M. Tönjes, S. Barbus, Y.J. Park, W. Wang, M. Schlotter, A.M. Lindroth, S. V Pleier, A.H.C. Bai, D. Karra, R.M. Piro, J. Felsberg, A. Addington, D. Lemke, I. Weibrecht, V. Hovestadt, C.G. Rolli, B. Campos, S. Turcan, D. Sturm, H. Witt, T.A. Chan, C. Herold-Mende, R. Kemkemer, R. König, K. Schmidt, W.-E. Hull, S.M. Pfister, M. Jugold, S.M. Hutson, C. Plass, J.G. Okun, G. Reifenberger, P. Lichter, B. Radlwimmer, BCAT1 promotes cell proliferation through amino acid catabolism in gliomas carrying wild-type IDH1, Nat. Med. 19 (2013) 901–908, https://doi.org/10.1038/nm.3217.

[24] M.E. Conway, S.J. Coles, M.M. Islam, S.M. Hutson, Regulatory control of human Cytosolic branched-chain aminotransferase by oxidation and S-Glutathionylation and its interactions with Redox sensitive neuronal proteins, Biochemistry 47 (2008) 5465–5479, https://doi.org/10.1021/bi800303h.

[25] S.J. Coles, P. Easton, H. Sharrod, S.M. Hutson, J. Hancock, V.B. Patel, M. E. Conway, S-Nitrosoglutathione inactivation of the mitochondrial and cytosolic BCAT proteins: S-nitrosation and S-thiolation, Biochemistry 48 (2009) 645–656, https://doi.org/10.1021/bi801805h.

[26] S.J. Coles, J.T. Hancock, M.E. Conway, Differential redox potential between the human cytosolic and mitochondrial branched-chain aminotransferase, Acta Biochim. Biophys. Sin. (Shanghai). 44 (2012) 172–176, https://doi.org/10.1093/abbs/gmr103.

[27] J. Hillier, G.J. Allcott, L.A. Guest, W. Heaselgrave, A. Tonks, M.E. Conway, A. L. Cherry, S.J. Coles, The BCAT1 CXXC motif provides protection against ROS in Acute Myeloid leukaemia cells, Antioxidants (Basel) 11 (2022), https://doi.org/10.3390/antiox11040683.

[28] L.S. Holliday, L.P. de Faria, W.J. Rody, Actin and actin-associated proteins in extracellular vesicles shed by osteoclasts, Int. J. Mol. Sci. 21 (2019), https://doi.org/10.3390/ijms21010158.

[29] K. Man, M.Y. Brunet, M. Fernandez-Rhodes, S. Williams, L.M. Heaney, L. A. Gethings, A. Federici, O.G. Davies, D. Hoey, S.C. Cox, Epigenetic reprogramming enhances the therapeutic efficacy of osteoblast-derived extracellular vesicles to promote human bone marrow stem cell osteogenic differentiation, J. Extracell. Vesicles 10 (2021), https://doi.org/10.1002/jev2.12118.

[30] P. Yang, Y. Peng, Y. Feng, Z. Xu, P. Feng, J. Cao, Y. Chen, X. Chen, X. Cao, Y. Yang, J. Jie, Immune cell-derived extracellular vesicles – new strategies in cancer immunotherapy, Front. Immunol. 12 (2021), https://doi.org/10.3389/fimmu.2021.771551.

[31] T. Wu, J.H.L. Tan, W. Sin, Y.H. Luah, S.Y. Tan, M. Goh, M.E. Birnbaum, Q. Chen, L. F. Cheow, Cell granularity reflects immune cell function and enables selection of lymphocytes with superior attributes for immunotherapy, Adv. Sci. 10 (2023), https://doi.org/10.1002/advs.202302175.

[32] T. Buchacher, A. Ohradanova-Repic, H. Stockinger, M.B. Fischer, V. Weber, M2 polarization of human macrophages favors survival of the intracellular pathogen Chlamydia pneumoniae, PLoS One 10 (2015) e0143593, https://doi.org/10.1371/journal.pone.0143593.

[33] L. Li, Y. Chen, S.B. Gibson, Starvation-induced autophagy is regulated by mitochondrial reactive oxygen species leading to AMPK activation, Cell. Signal. 25 (2013) 50–65, https://doi.org/10.1016/j.cellsig.2012.09.020.

[34] L.W. Schultz, P.T. Chivers, R.T. Raines, The C *XX* C motif: crystal structure of an active-site variant of *Escherichia coli* thioredoxin, Acta Crystallogr. D Biol. Crystallogr. 55 (1999) 1533–1538, https://doi.org/10.1107/S0907444999008756.

[35] V. Syromiatnikova, A. Prokopeva, M. Gomzikova, Methods of the large-scale production of extracellular vesicles, Int. J. Mol. Sci. 23 (2022) 10522, https://doi.org/10.3390/ijms231810522.

[36] K.D. Little, M.E. Hemler, C.S. Stipp, Dynamic regulation of a GPCR-tetraspanin-G protein complex on intact cells: central role of CD81 in facilitating GPR56-Galpha q/11 association, Mol. Biol. Cell 15 (2004) 2375–2387, https://doi.org/10.1091/mbc.e03-12-0886.

[37] B. Wu, J. Liu, R. Zhao, Y. Li, J. Peer, A.L. Braun, L. Zhao, Y. Wang, Z. Tong, Y. Huang, J.C. Zheng, Glutaminase 1 regulates the release of extracellular vesicles during neuroinflammation through key metabolic intermediate alpha-ketoglutarate, J. Neuroinflammation 15 (2018) 79, https://doi.org/10.1186/s12974-018-1120-x.

[38] W. Zou, M. Lai, Y. Zhang, L. Zheng, Z. Xing, T. Li, Z. Zou, Q. Song, X. Zhao, L. Xia, J. Yang, A. Liu, H. Zhang, Z. Cui, Y. Jiang, X. Bai, Exosome release is regulated by mTORC1, Adv. Sci. 6 (2019), https://doi.org/10.1002/advs.201801313.

[39] B. Pang, G. Dong, T. Pang, X. Sun, X. Liu, Y. Nie, X. Chang, Advances in pathogenesis and treatment of vascular endothelial injury-related diseases mediated by mitochondrial abnormality, Front. Pharmacol. 15 (2024) 1422686, https://doi.org/10.3389/fphar.2024.1422686.

[40] J. Wang, H. Zhuang, C. Li, R. Cai, H. Shi, B. Pang, Z. Guo, S.-B. Ong, Y. Nie, Y. Du, H. Zhou, X. Chang, Ligustrazine nano-drug delivery system ameliorates doxorubicin-mediated myocardial injury via piezo-type mechanosensitive ion channel component 1-prohibitin 2-mediated mitochondrial quality surveillance, J. Nanobiotechnol. 23 (2025) 383, https://doi.org/10.1186/s12951-025-03420-z.

[41] X. Pu, Q. Wu, Z. Yan, S. Zhou, Q. Zhang, X. Zhang, Y. Cai, Z. Liu, R. Liu, X. Chang, Tanshinone IIA modulates Sirt5 and Metll3 interaction to govern mitochondria-endoplasmic reticulum unfolded protein response in coronary microvascular injury, Phytomedicine 145 (2025) 156982, https://doi.org/10.1016/j.phymed.2025.156982.

[42] X. Chang, H. Zhou, J. Hu, T. Ge, K. He, Y. Chen, R. Zou, X. Fan, Targeting mitochondria by lipid-selenium conjugate drug results in malate/fumarate exhaustion and induces mitophagy-mediated necroptosis suppression, Int. J. Biol. Sci. 20 (2024) 5793–5811, https://doi.org/10.7150/ijbs.102424.

[43] X. Chang, S. Zhou, Z. Yan, Q. Zhang, J. Liu, Y. Wang, X. Guan, Q. Wu, R. Liu, Potential candidates of natural antioxidants from herbs for treating lung disorders: focus on redox balance and natural products, Phytother. Res. 39 (2025) 3353–3385, https://doi.org/10.1002/ptr.70008.

[44] P. Italiani, D. Boraschi, From monocytes to M1/M2 macrophages: phenotypical vs. functional differentiation, Front. Immunol. 5 (2014), https://doi.org/10.3389/fimmu.2014.00514.

[45] D.M. Mosser, J.P. Edwards, Exploring the full spectrum of macrophage activation, Nat. Rev. Immunol. 8 (2008) 958–969, https://doi.org/10.1038/nri2448.

[46] A.R. Nager, J.S. Goldstein, V. Herranz-Pérez, D. Portran, F. Ye, J.M. Garcia-Verdugo, M.V. Nachury, An actin network dispatches ciliary GPCRs into extracellular vesicles to modulate signaling, Cell 168 (2017) 252–263.e14, https://doi.org/10.1016/j.cell.2016.11.036.

[47] L.S. Holliday, L.P. de Faria, W.J. Rody, Actin and actin-associated proteins in extracellular vesicles shed by osteoclasts, Int. J. Mol. Sci. 21 (2019) 158, https://doi.org/10.3390/ijms21010158.

[48] P. Goyal, D. Pandey, D. Brünnert, E. Hammer, M. Zygmunt, W. Siess, Cofilin oligomer formation occurs in vivo and is regulated by cofilin phosphorylation, PLoS One 8 (2013) e71769, https://doi.org/10.1371/journal.pone.0071769.

[49] Q. Wu, Y. Wang, J. Liu, X. Guan, X. Chang, Z. Liu, R. Liu, Microtubules and cardiovascular diseases: insights into pathology and therapeutic strategies, Int. J. Biochem. Cell Biol. 175 (2024) 106650, https://doi.org/10.1016/j.biocel.2024.106650.

[50] M. Daigneault, J.A. Preston, H.M. Marriott, M.K.B. Whyte, D.H. Dockrell, The identification of markers of macrophage differentiation in PMA-stimulated THP-1

cells and monocyte-derived macrophages, PLoS One 5 (2010) e8668, https://doi.org/10.1371/journal.pone.0008668.
[51] P. Krzyszczyk, R. Schloss, A. Palmer, F. Berthiaume, The role of macrophages in acute and chronic wound healing and interventions to promote pro-wound healing phenotypes, Front. Physiol. 9 (2018), https://doi.org/10.3389/fphys.2018.00419.
[52] X. Wu, W. He, X. Mu, Y. Liu, J. Deng, Y. Liu, X. Nie, Macrophage polarization in diabetic wound healing, Burns Trauma 10 (2022), https://doi.org/10.1093/burnst/tkac051.
[53] H. Shi, B. Pang, F. Zhang, Z. Guo, W. Xu, M. Zheng, Y. You, G. Liu, Y. Nie, J. Liang, X. Chang, A novel ligustrazine-based nanodelivery system protects against doxorubicin-induced cardiotoxicity by targeting the SIRT5-DUSP1 axis for mitochondrial repair, J. Nanobiotechnol. 23 (2025) 681, https://doi.org/10.1186/s12951-025-03667-6.